Numerical study of geometrical dispersion in self-affine rough fractures

Franck Plouraboué,[1] Jean-Pierre Hulin,[2] Stéphane Roux,[3] and Joel Koplik[4]
[1]*Institut de Mécanique des Fluides, UMR CNRS No. 5502, Allée du Pr. C. Soula, 31400 Toulouse, France*
[2]*Laboratoire Fluide, Automatique et Systèmes Thermiques, URA CNRS No. 871 Bâtiment 502, Université Paris–Sud, 91405 Orsay, France*
[3]*Laboratoire ''Surface du Verre et Interfaces,'' UMR CNRS St. Gobain No. 125, 39 Quai L. Lefranc, Boîte Postale 135, F-93303 Aubervilliers Cédex, France*
[4]*Benjamin Levich Institute and Department of Physics, City College of the City University of New York, New York, New York 10031*
(Received 20 January 1998)

We report a numerical study of passive tracer dispersion in fractures with rough walls modeled as the space between two complementary self-affine surfaces rigidly translated with respect to each other. Geometrical dispersion due to the disorder of the velocity distribution is computed using the lubrication approximation. Using a spectral perturbative scheme to solve the flow problem and a mapping coordinate method to compute dispersion, we perform extensive ensemble averaged simulations to test theoretical predictions on the dispersion dependence on simple geometrical parameters. We observe the expected quadratic dispersion coefficient dependence on both the mean aperture and the relative shift of the crack as of well as the anomalous dispersion dependence on tracer traveling distance. We also characterize the anisotropy of the dispersion front, which progressively wrinkles into a self-affine curve whose exponent is equal to that of the fracture surface. [S1063-651X(98)05009-0]

PACS number(s): 62.20.Mk, 05.40.+j

I. INTRODUCTION

A. Motivation of the study

Flow and mass transport in fractured media is a complex problem with many applications to pollutant dispersion and waste storage as well as to geothermic and oil and gas recovery processes [1,2]. From a fundamental point of view, it has recently stimulated a great deal of interest in connection with different approaches to the description of fracture roughness in terms of a self-affine geometry [3,4]. A key observation [5,6] is that flow and solute transport are not distributed evenly across the fracture surface: Instead, they are often concentrated in some preferential flow paths while large parts of the fracture often act as dead zones. This effect is very much dependent on the roughness of the fracture walls and it plays a crucial role in enhancing pollutant transport in a fractured zone.

In the present paper we present a numerical simulation of tracer dispersion in fractures with self-affine rough walls. Tracer dispersion, due to its nonlocal nature [7,8], is indeed a unique tool used to detect and characterize the influence of preferential flow channels: Particles flowing through such paths cross the sample and reach the detectors much sooner than those trapped inside low-velocity zones. More global measurements such as the average permeability or electrical conductivity of the fracture are dominantly controlled by its effective aperture [9] and thus are less sensitive to flow heterogeneities. Previous studies have indeed confirmed that tracer dispersion in fracture geometries [5,10,11] often results largely from disparities between transit times along macroscopic parallel flow channels.

The present work is devoted to a systematic quantitative numerical analysis of these problems in the realistic case of a self-affine roughness geometry. We investigate in particular the influence of the sample size, of the relative displacement of the complementary rough walls, and of the orientation between the mean flow and the displacement. The simulations are two-dimensional, involving a two-dimensional fracture surface, and the flow is computed in the lubrication approximation. Let us discuss now the dispersion mechanisms acting in fractures and their domain of applicability.

B. Tracer dispersion mechanisms in rough fractures

Tracer dispersion is a key tool used to analyze nonlocal spatial correlations of the velocity field in a porous or fractured system. We consider a steady three-dimensional Stokes flow $\vec{u}(x)$ established in the rough wall fracture geometry introduced above. Locally, we assume that the local tracer concentration c obeys a convection-diffusion equation

$$\frac{\partial c(\vec{x},t)}{\partial t}+\vec{u}(\vec{x})\cdot\vec{\nabla}c(\vec{x},t)=D_m\nabla^2 c(\vec{x},t), \tag{1}$$

where D_m is the molecular diffusion coefficient. This behavior is *postulated* at the local level.

Our aim is to be able to characterize the dispersion properties of the tracer in such a geometry without having to resort to a detailed three-dimensional description. Upon coarse graining at a scale much larger than the heterogeneity scale and integration over the thickness x_3 of the crack, it can be shown that if the heterogeneity is small enough, the coarse-grained concentration $C(x_1,x_2)$ obeys an effective convection-diffusion equation, with the coarse-grained velocity $\vec{U}(x_1,x_2)$ giving the advection term and an effective dispersivity tensor D_{ij}.

We define the coarse-grained fields as

$$C(x_1,x_2)=\int\int \varphi(x_1-x_1',x_2-x_2') \times\left((1/h)\int c(x_1',x_2',x_3')dx_3'\right)dx_1'dx_2', \quad (2)$$

where h is the aperture of the crack and φ is the coarse-graining weight function, e.g., a Gaussian, of unit integral and decaying fast above a typical length scale larger than the heterogeneity scale. A similar transformation is made on the velocity field. The macroscopic description can be written as [7]

$$\frac{\partial C}{\partial t}+U_i\frac{\partial C}{\partial x_i}=D_{ij}\frac{\partial^2 C}{\partial x_i\partial x_j}. \quad (3)$$

U_i and D_{ij} are, respectively, the components of the local mean macroscopic flow velocity through the fracture or the porous sample (averaged over the aperture) and of the dispersivity tensor. The latter dispersivity tensor results from velocity fluctuations in the local field and/or systematic variation across the thickness, which are absent from the coarse-grained description. D can be expressed as the Lagrangian velocity field covariance tensor [12]

$$D_{ij}=\lim_{T\to\infty}\left\langle \int_0^T [V_i(0)-U_i][V_j(t)-U_j]dt \right\rangle, \quad (4)$$

where the integration is performed over particule trajectories and V is the two-dimensional velocity field obtained from an integration of $\vec{u}$ over the aperture.

Several dispersion mechanisms are present in fractures. Let us first discuss the ideal case of a perfect Hele-Shaw cell, i.e., an ideal plane crack with a constant aperture h, and an uniform flow. In this case, the velocity is simply a Poiseuille flow with a parabolic profile across the thickness. The coarse graining in this simple case consists in averaging the velocity components over the thickness. Pure molecular diffusion is significant only at extremely low velocities such that the Péclet number $\mathrm{Pe}=Uh/D_m$ is less than 1. At high velocities, the Taylor dispersion mechanism [13] dominates: It accounts for the spreading due to the Poiseuille velocity profile between the fracture walls balanced by transverse molecular diffusion (homogenizing tracer concentration across the aperture). The resulting longitudinal ''Taylor'' dispersion coefficient $D_\parallel$ can be obtained analytically in this case for parallel plane walls as [14]

$$D_\parallel=D_{Taylor}=\frac{h^2U^2}{210D_m}+D_m \quad (5)$$

($D_\parallel$ is the longitudinal dispersivity coefficient, i.e., D_{xx} for a flow along the x axis). Taylor dispersion is observable in fractures because of their inherently quasi-two-dimensional flow geometry: Only molecular diffusion can move tracer particles across the flow lines away from the fracture walls or towards them. On the contrary, in usual random three-dimensional porous media such as grain packings, a given flow line moves continuously away from pore walls or towards them along its path through severals pores; hence Taylor dispersion does not play such an important part. Molecular diffusion and Taylor dispersion are the only two mechanisms active in fractures with smooth plane walls.

For rough walls, on the contrary, the aperture of the crack is no longer constant and therefore the fluid velocity displays spatial fluctuations even after being averaged over the thickness. This additional mechanism is also assumed to be taken into account in the coarse description, corresponding to a scale much larger than the heterogeneity scale. It induces a geometrical dispersion component, an effect comparable to that observed in three-dimensional porous media [7,15]). If Eq. (3) is satisfied, the longitudinal coefficient $D_\parallel$ is proportional to velocity (the dispersivity $\ell_D=D_{//}/U$ represents the Lagrangian correlation length of the flow field). The geometrical, molecular, and Taylor dispersion components simply add up in series: Thus the U^2 Taylor dispersion component dominates at high velocities, geometrical (U) dispersion at lower ones, and finally (U^0) molecular diffusion at still lower velocities. A quantitative theoretical analysis of the expected transition between these different regimes can be found in [16] as well as predictions of the dependence of the geometrical regime on the roughness of the crack. These predictions are verified qualitatively in experiments [17] on model fractures with parallel plane walls: For smooth surfaces, only molecular and Taylor dispersion are observed; for rough ones, geometrical dispersion occurs at low velocities and the Taylor component dominates at higher ones.

The present numerical model deals with geometrical dispersion effects directly associated with the velocity field disorder; Taylor and molecular dispersion terms are, on the contrary, much less related to flow field heterogeneities and are not taken into account. We can thus use a simpler two-dimensional model since we do not need to take into account the flow structure in the direction perpendicular to the fracture surface. These simulations describe adequately tracer dispersion in the intermediate range of Péclet number values such that both molecular diffusion and Taylor dispersion are negligible. The limit of validity increases towards higher Pe values as the heterogeneity of the flow field increases for a given mean fracture aperture: Geometrical dispersion, indeed increases with heterogeneity and ends up superseding Taylor dispersion which remains almost the same. It must be also pointed also that the Gaussian convection-diffusion equation (3) is valid only if the correlation length of the flow velocity field is small compared to the sample size: This is not the case when large-scale preferential channels are present and dispersion must then be characterized in another way.

C. Geometrical and transport properties of self-affine rough fracture joints

An important point in modeling the topography of fracture surfaces is the observation that they can often be described as self-affine structures [3]: This applies to very diverse materials (for instance, metal alloys, concrete, rocks such as granite [18,19], marble, and sandstone [20]). Self-affine surfaces display scale invariant properties provided one uses different dilation ratios parallel λ_1, λ_2 and perpendicular λ_3 to the mean fracture plane, related by

$$\lambda_3=\lambda_{(1,2)}^{\zeta} \quad (6)$$

(ζ is called the Hurst exponent). This property implies the

existence of long-range correlations in the geometrical structure of the fracture surface: These in turn give rise to length scale effects that must be understood and taken into account when extrapolating laboratory scale measurements to field applications. Such characteristics are observed for very diverse materials and fracturation mechanisms; the exponent ζ has also been found in many cases to be close to a same value $\zeta = 0.8 \pm 0.05$, although some deviations have been observed for some materials and at some length scales.

It has been suggested [4] that these self-affine features allow one to predict variations of geometrical and transport properties for fractures limited by complementary surfaces shifted with respect to each other. A an important ingredient is the residual displacement Δz perpendicular to their mean plane of two such surfaces of global size L after they have been displaced laterally by a distance Δx. It has been shown [18] both experimentally (on granite blocks) and theoretically that Δz does not scale exactly as expected as Δx^{ζ}, but that a logarithmic finite size term depending on the ratio $\Delta x/L$ must be introduced. Global physical quantities such as the permeability of the fracture or its effective electrical conductance after it has been saturated with a conducting fluid have also been studied [9]. Both the permeability and the electrical conductances are shown to depend mostly on the normal distance Δz, however, very large fluctuations of these quantities are observed when the direction and the amplitude of the lateral displacement Δx is varied, Δz being kept constant. This confirms that the flow velocity and the electrical current fields are influenced by the displacement and that strong heterogeneities may appear: tracer dispersion should be much more sensitive to these effects.

Previous numerical simulations [21,22] have been performed to investigate the influence of random or self-affine roughness on tracer dispersion through fractures: It is assumed in these works that the local fracture thickness remains constant in the direction perpendicular to the flow in the fracture plane. This allows one to describe in detail the influence of roughness on Taylor dispersion; however, it is impossible in this framework to account for geometrical dispersion effects that require thickness variations in the two directions of the mean fracture plane. Other authors [10,11,5,23] have studied flow in fractures simulated as a random permeability field accounting for aperture variations. They did not, however, introduce specific aspects related to the self-affine roughness geometry or to the fact that we are not dealing with independent rough surfaces but with identical surfaces shifted by a specific amount. This mirrors the fact that actual fractures observed in nature are created from a single block of material [24] with the two halves shifted thereafter by external stresses. It has been shown theoretically [18] that, in this case, the correlation between the aperture at two different points of the fracture depends strongly on the relative displacement of the surfaces: This will obviously influence the structure of the flow field. We shall therefore pay particular attention to the influence on tracer dispersion of this relative shift and of its orientation; the influence of the finite size effects discussed above on the magnitude of dispersion will also be investigated.

II. NUMERICAL METHODS

Our aim is to take into account the multiscale features of the crack permeability induced by the crack roughness. As mentioned in the Introduction, we focus here on case of self-affine topography, observed in many instances. We first generate a self-affine surface with biperiodic boundary conditions. We used both a dichotomy algorithm introduced by Voss [25] and a Fourier method to generate such a self-affine topography. The roughness exponent is chosen to be $\zeta = 0.8$. The amplitude of the roughness is chosen so that the mean value of the height difference at the mesh size of the discretization is constant. Therefore, the global standard deviation of the height of the crack depends on its size L. The crack surface $z(x)$ is then used to compute the aperture of the crack after the two faces are translated with respect to each other by a shift along the mean crack plane u, plus a translation h normal to the mean plane so that the two surfaces do not overlap but have a point of contact. Therefore, we obtain the aperture field as $a(x) = z(x) - z(x+u) + h$.

Given the aperture field, we use the lubrication or Reynolds approximation to compute the velocity field. Thus we consider the aperture gradient to be small enough so that we may consider that the velocity field is locally a Poiseuille flow everywhere in the crack, with a parabolic velocity profile across the aperture. This reduces the three-dimensional problem to a two-dimensional one and we simply have to determine the aperture-averaged velocity field $\vec{v}$ from (i) the incompressibility condition

$$\vec{\nabla} \cdot [a(\vec{x})\vec{v}(\vec{x})] = 0 \tag{7}$$

and (ii) the flux/pressure relation similar to Darcy's law, with a local permeability proportional to the square of the aperture

$$v(\vec{x}) = -\frac{a^2(\vec{x})}{12\eta}\vec{\nabla} P(\vec{x}) = -\frac{k(\vec{x})}{\eta}\vec{\nabla} P(\vec{x}), \tag{8}$$

where P is the coarse-grained pressure field. The applicability of the Reynolds approximation is based on the condition that the aperture gradient is much smaller than unity, i.e., $|\vec{\nabla} a| \ll 1$. In turn, this implies that the local slope of the crack surface is much smaller than unity. Let us note that in the case of a self-affine crack, with a roughness exponent strictly smaller than unity, the coarse-grained slope estimated at a scale ℓ decreases as $\ell^{\zeta - 1}$. Therefore, the small slope limitation can be used at a sufficiently coarsened scale if an effective hydraulic aperture is introduced. Using an experimental determination of the crack surface topography, the Reynolds approximation has been shown to be valid above a scale of a few series of 10 μm [9].

The numerical solution proceeds in two steps. One first solves for the pressure and stream function. Then tracer advection is computed in the pressure-stream function coordinate system and the corresponding spreading of a tracer step profile is computed from the advection time along streamlines.

A. Hydraulic solution

Given the permeability field $k(\vec{x})$ on a squared $L \times L$ meshed domain D, the pressure field $P(\vec{x})$ satisifes the equation imposed by the divergence-free flux field and the local Darcy relation (8):

$$\Delta P(\vec{x}) = -\frac{3}{2}\frac{\vec{\nabla}k(\vec{x})}{k(\vec{x})}\cdot\vec{\nabla}P(\vec{x}) = -\frac{3}{2}\vec{\nabla}[\ln k(\vec{x})]\cdot\vec{\nabla}P(\vec{x}). \tag{9}$$

From the definition of the stream function $\vec{\Psi}(\vec{x}) = (0,0,\Psi(\vec{x}))$, $a(\vec{x})\vec{v}(\vec{x}) = \vec{\nabla}\times\vec{\Psi}(\vec{x})$, and Darcy's law (8) we get

$$\Delta\Psi(\vec{x}) = \frac{3}{2}\frac{\vec{\nabla}k(\vec{x})}{k(\vec{x})}\cdot\vec{\nabla}\Psi(\vec{x}) = \frac{3}{2}\vec{\nabla}[\ln k(\vec{x})]\cdot\vec{\nabla}\Psi(\vec{x}), \tag{10}$$

with

$$\vec{\nabla}P(\vec{x})\cdot\vec{\nabla}\Psi(\vec{x}) = 0.$$

These two very similar equations can be solved, simultaneously and iteratively, by a spectral method consistent with the biperiodicity of the permeability field. This choice is numerically convenient in the sense that it limits the spurious effects of boundary conditions. However, its weakness lies in the absence of an experimental counterpart.

We note that if the pressure gradient is periodic, the pressure itself is not periodic but can be split into a periodic part and a constant gradient term. The latter is treated separately and acts as the forcing term for the flow. The mean pressure gradient is oriented at 45° with respect to the principal axis of the square grid used in the discretization, in order to limit mesh orientation effects. The spectral iterative procedure is based on a weak disorder expansion, commonly encountered in heterogeneous porous media literature [7]. The following procedure, albeit restricted to weakly heterogeneous media unlike Ref [26], is consistent with the aperture field of realistic fractures [9]. From Eq. (9) we look for a solution for the pressure gradient in the form of an expansion

$$\vec{\nabla}P(x) = \vec{\nabla}P^{(0)}(x) + \vec{\nabla}P^{(1)}(x) + \cdots + \vec{\nabla}P^{(n)}(x) + \cdots, \tag{11}$$

where

$$\Delta P^{(0)}(x) = 0 \tag{12}$$

for

$$n>0\,\Delta P^{(n)}(x) = -\frac{3}{2}\vec{\nabla}[\ln k(x)]\cdot\vec{\nabla}P^{(n-1)}(x).$$

The zeroth-order solution corresponds to the imposed constant mean pressure gradient, i.e., $\vec{\nabla}P^0(x) = \vec{\nabla}P^0$. Each consecutive term is computed with a standard pseudospectral technique. We compute on the right-hand side the scalar product in direct space, while Laplacian inversion is calculated in Fourier space on the left-hand side. The use of the fast Fourier transform algorithm makes this procedure very efficient compared to direct-space conjugate gradient techniques. A sufficient condition for such spectral iterative procedure to converge is $\frac{3}{2}\vec{\nabla}\ln k(x)\cdot\vec{\nabla}P^0/\|\vec{\nabla}P^0\| < 1$ for every position x, provided the greater eigenvalue associated with the iterated pressure solution is always 1. A less restrictive condition can be obtained with an underrelaxation iterative scheme. Such an underrelaxation can even be imposed locally, i.e., precisely in the region where $\frac{3}{2}\vec{\nabla}\ln k(x)\cdot\vec{\nabla}P^0/\|\vec{\nabla}P^0\| > 1$, for greater efficiency.

B. Tracer dispersion

Once the pressure and velocity fields are determined, we wish to model the *geometrical dispersion regime*. For that purpose, we note that the parabolic velocity profile is an essential ingredient of the Taylor regime, but that it does not affect the geometrical dispersion. We assume that molecular diffusion is efficient enough to avoid the Taylor regime, i.e., $Ua/D_m < 1$. This allows us to deal simply with the aperture-averaged velocity field (i.e., a two-dimensional description in the mean crack plane). It is assumed that aperture variations occur over much larger scales than the mean aperture and the velocity is large enough to have convection effects dominant compared to diffusion ones. For this discussion, we introduce the ''Péclet'' number Pe′ constructed from the velocity fluctuation δV and the correlation length of the aperture fluctuation ξ so that $\mathrm{Pe}' = \delta V\xi/D_m$. To observe the geometric dispersion regime we assume $\mathrm{Pe}' \gg 1$. In this limit, valid only for $\xi \gg h$, we can consider the ''infinite'' Péclet number limit of the two-dimensional description. More precisely, using our previously defined Péclet number $\mathrm{Pe} = Uh/D_m$, we obtained in [16] the limit of validity of the geometrical regime

$$\left(\frac{\delta V}{U}\right)^{-2}\frac{h}{\xi} \ll \mathrm{Pe} \ll \left(\frac{\delta V}{U}\right)^{2}\frac{\xi}{h}. \tag{13}$$

It must be stressed that such a limiting condition is needed when there is a well defined correlation length for the velocity field. We expect a less restrictive condition in the presence of long-range correlations of the velocity field as examined here. It is also important to note that this limit is different from the infinite Péclet limit of the full three-dimensional problem, which is evidently governed by the Taylor regime.

To compute tracer dispersion in the geometric regime, we have to study the transit time distribution for particles passively advected across the domain by the fluid flow. In order to follow the particle trajectories we use a coordinates change from Cartesian (x,y) position to an adimensionalized pressure-stream function $(P(x,y),\Psi(x,y))$ orthogonal coordinate system. This procedure is interesting because it overcomes numerical problems currently encountered with direct Lagrangian computation of particle trajectories, such as locally nondivergent free velocity fields coming from a continuous interpolation of the discrete flow field. Such effects, although localized at the mesh size scale, are accumulated over the particles' trajectories and can lead to spurious violations of the periodicity of the tracer spatial distribution in the case of periodic boundary conditions. The idea of the present method is to compute the trajectories of particles as a change of coordinates. A mandatory condition for such a coordinate mapping to exist is the bijectivity of the maping between the coordinates (x,y) and the pressure streamfunction $(P(x,y),\Psi(x,y))$ pair. This condition is fulfilled for a strictly monotonic pressure in the direction of the mean imposed flow and a strictly monotonic stream function perpendicular to this direction. This is obtained, in our case in

the presence of a mean imposed pressure gradient, for weakly heterogeneous media. More precisely, for such medium, each consecutive nth term of the pressure expansion written in Eq. (11) can be shown [27,7] to be of $O(\sigma^{2n}(\ln k))$, where $\sigma(\ln k)$ is the log-permeability fluctuation parameter. A weak disorder expansion (9) can be written if $\sigma(\ln k) \ll 1$, which gives a sufficient condition to impose a strictly monotonic pressure and stream function for a log-normal permeability field distribution. Practically, for fresh, noncompressed fractures, relative fluctuations of the aperture field are sufficiently weak [9] to allow for such a coordinate mapping. Hence one is interested in inverting the $(P(x,y),\Psi(x,y))$ relation to find the $(x(P,\Psi),y(P,\Psi))$ positions of pressure and stream-function isovalues. To simplify notations, we introduce the normalized stream-function

$$\psi(x,y)=\Psi(x,y)/\langle k\rangle, \tag{14}$$

where $\langle k\rangle$ is the arithmetic mean of the permeability field. This choice provides symmetrical expression for the pressure and the normalized stream function. At the zeroth order of perturbation expansion the Darcy law (8) can be rewritten $\vec{\nabla}\times\vec{\psi}^0=\vec{\nabla}P^0$. This relation can be inverted numerically by an iterative procedure. We will write for convenience this inversion with a mean pressure gradient parallel to x axis. We choose a mean pressure gradient parallel to the principal diagonal direction for numerical precision

$$P(x,y)=x+f(x,y), \tag{15}$$

$$\psi(x,y)=y+g(x,y).$$

The functions f and g are known from the numerical solution of Eqs. (9) and (10). We are now interested in finding the inverse mapping

$$x(P,\psi)=P+X(P,\psi), \tag{16}$$

$$y(P,\psi)=\psi+Y(P,\psi),$$

where $X(P,\psi),Y(P,\psi)$ are the desired inverse mapping functions. From Eqs. (15) and (16) we obtain the implicit equation satisfied by $X(P,\psi)$ and $Y(P,\psi)$,

$$X(P,\psi)=-f(P+X,\psi+Y)=-f, \tag{17}$$

$$Y(P,\psi)=-g(P+X,\psi+Y)=-g.$$

The computation of $X(P,\psi),Y(P,\psi)$ is achieved in the same spirit as Eq. (9) with an iterative procedure. First, we approximate the right-hand side dependence of $f(x,y)$ and $g(x,y)$ by $f(P,\psi)$ and $g(P,\psi)$,

$$X^0(P,\psi)=0, \tag{18}$$

$$Y^0(P,\psi)=0.$$

We then proceed iteratively for $n>0$,

$$X^n(P,\psi)=-f(P+X^{n-1},\psi+Y^{n-1}), \tag{19}$$

$$Y^n(P,\psi)=-g(P+X^{n-1},\psi+Y^{n-1}).$$

The convergence of this method is conditioned by the Jacobian $J(x,y)_{\{P,\Psi\}}$ of the transformation (16). It is straightforward to show that this Jacobian satisfies

$$J^{-1}(x,y)_{\{P,\psi\}}=\vec{\nabla}P\cdot\vec{\nabla}\times\vec{\psi}=\|\vec{\nabla}P\|^2\frac{a(x)^3}{12\eta}. \tag{20}$$

Computing Eq. (16) thus requires that at each (x,y) location $\|J(x,y)_{\{P,\Psi\}}\|\leqslant 1$. As can be seen from Eq. (20), this condition is fulfilled in a weakly disordered system, where the local dissipated energy is dominated by the mean imposed $\vec{\nabla}P^0\cdot\vec{\nabla}\times\vec{\psi}^0$. Numerical implementation of this iterative procedure requires, at each step, the estimation $X^n(P,\psi),Y^n(P,\psi)$ on the continuous system of coordinates (P,ψ), from the values of f and g on a discrete one. This estimation is achieved with an undermesh mapping, to interpolate linearly an accurate estimation of the continuous desired $X^n(P,\psi),Y^n(P,\psi)$. Dispersion curves are then easily computed in the (P,ψ) coordinate system, integrating the advection time along each streamline $\psi(x,y)=c$.

III. NUMERICAL RESULTS

A. Stream-function structure

The aperture maps of Figs. 1(a) and 1(b) show the influence of the relative shift d of crack faces on the typical correlation length of the permeability field. The aperture field is coded with gray levels from white for maximal aperture to black for complete contact. The influence of the relative joint shift d on the streamlines is illustrated in Figs. 1(c) and 1(d). These figures represent with bold lines stream-function isovalues computed solving (10) using the iterative procedure (11) and (12) on two periods in the x and y directions. These isovalues are to be compared with the computed pressure-stream-function orthogonal coordinates system represented on the deformed mesh computed from the scheme (18) and (19). These figures illustrate that the streamlines' large-scale features are mainly controled by the shift value. More precisely, the translation distance d between both faces defines an upper length scale cutoff for the streamlines' tortuosity. This qualitative observation is fully consistent with a previous analysis [18,16], showing that the multiscale aperture field cutoff length is precisely the distance d. As shown in Fig. 2, the translation d is the typical correlation length of the aperture covariance. Moreover, the choice of a direction of translation $\vec{d}$ leads to an anisotropy of the covariance. Figure 2 shows both the parallel and perpendicular (with respect to the in-plane displacement) covariance functions. Dispersion will appear to be strongly influenced by the streamline structure as shown in the following. Moreover, anisotropy, which is a natural consequence of our geometrical model, can also influence dispersion [28].

B. Geometrical influence on tracer transit time dispersion curves

In the ideal case of an uncorrelated velocity field, the transit time distribution is expected to be Gaussian, solely characterized by its mean value T and its variance $\Delta T^2=\overline{(t-T)^2}$. We define the dispersivity D through

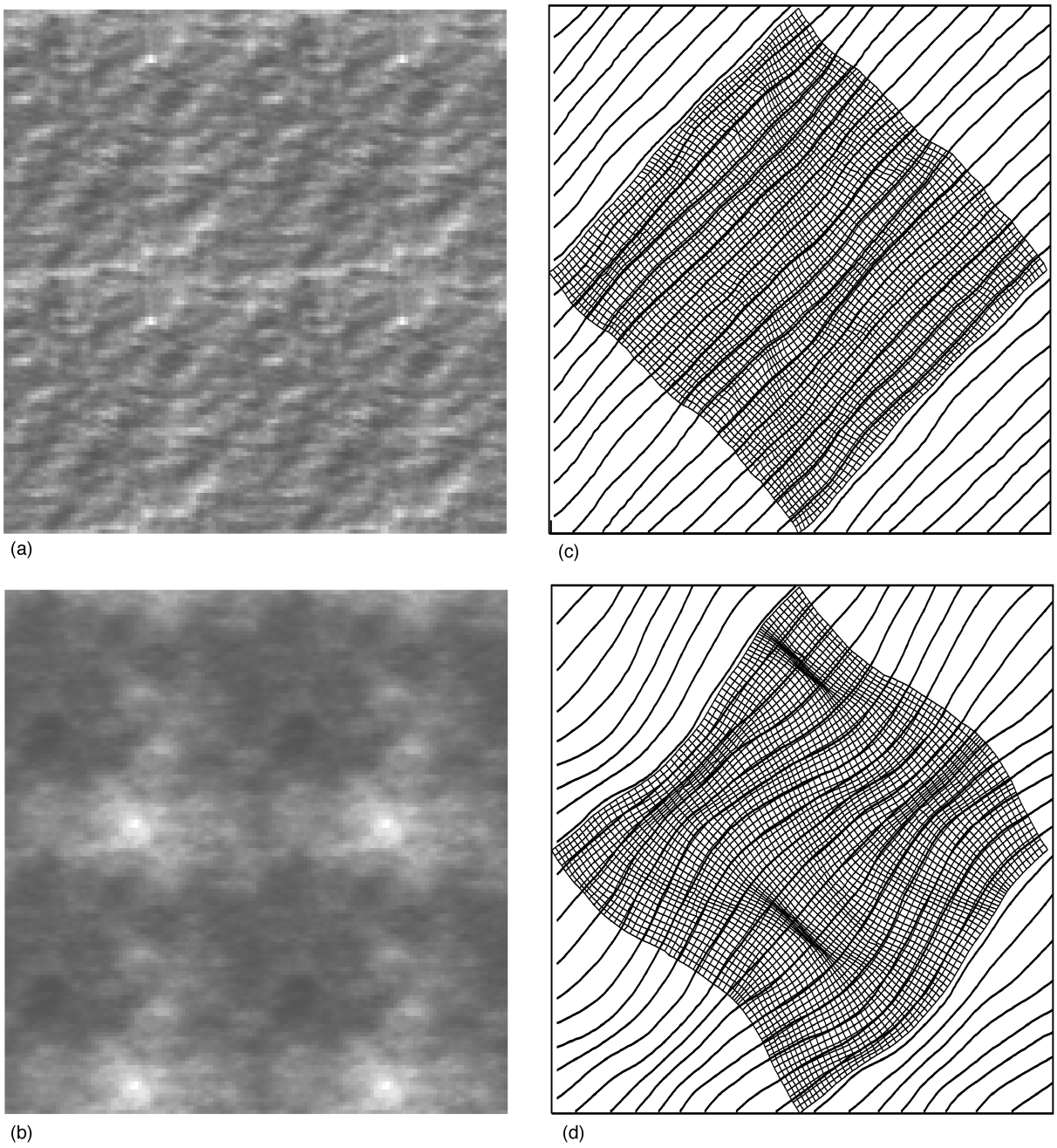

FIG. 1. Aperture field and corresponding computed streamlines for a 512×512 domain, with roughness exponent $\zeta=0.8$, pressure imposed, and no flux boundary conditions; (a) aperture field for a translation $d=128$ between crack faces in a gray scale, (b) aperture field for $d=32$ with the same crack surface topography as (a), (c) stream lines for permeability field a, and (d) streamlines for permeability field b.

$$D=\frac{\Delta T^2}{T^2}. \tag{21}$$

D is related to the dispersion coefficient $\mathcal{D}$, estimated at distance L_1 from the origin, in the presence of a mean velocity field U, $\mathcal{D}=L_1UD$. In the case considered in this work, the crack-face shift d is the typical correlation length. There is a finite number L/d of such a correlation length. The fact that this number L/d is rather limited in our case is one obvious cause for a deviation from a Gaussian distribution. Moreover, above the scale d, the aperture field is not completely uncorrelated. The covariance function decays with the distance as a power law with an exponent $-2(1-\zeta)$ and it can be shown that this decay is sufficient to induce an anomalous dispersion of the tracer for persistent crack topographies ($\zeta>0.5$). Tracer curves are obtained from the computation of the traveling time along streamlines. We illustrate in Fig. 3 the numerical estimate of the influence of finite size effects of the discretization mesh on tracer curve results. This influence on dispersion curves is quite small and validate the choice of size $L=128$ above which numerical results can be compared to theoretical predictions. Figure 4(a) shows tracer curves for the same crack surface

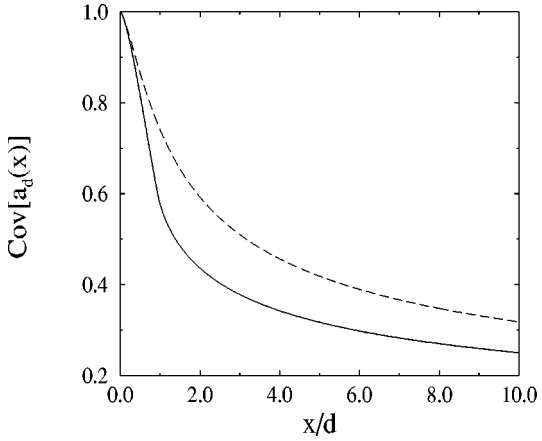

FIG. 2. Aperture covariances versus the normalized distance x/d for a self-affine crack of rough exponent $\zeta=0.8$ in the directions perpendicular (dashed line) and parallel (continuous line) to the translation direction.

for two different relative shift $d/L=1/128$ and 64/128. Gaussian and Coats-Smith [29] fits are shown for comparison, illustrating the non-Gaussian character of the transit time distribution. Although the Coats-Smith expression provides a reasonable fit to the data, we do not believe that the underlying theory is relevant to our case. We simply use it here as a measurement of the deviation from normal dispersion. Figure 4(b) shows a superposition of each reduced-centered exit time distributions. It indicates a small sensitivity of the higher moments (>2) of the tracer exit time distribution to the shift d of the two crack surfaces. This numerical result leads us to focus on the second moment (which should survive at long time scales in the absence of correlations) However, we have recently been able to develop, in a previous analysis [16], a more refined description of the tracer front useful for estimating *local* dispersion. This dispersion is obtained by measuring tracer spreading at a particular point and is generally much easier to perform than global measurements integrated over a line of tracer. The latter dispersion, which is relevant for both field and experimental purposes, is sensitive to the spatial correlation of the tracer front.

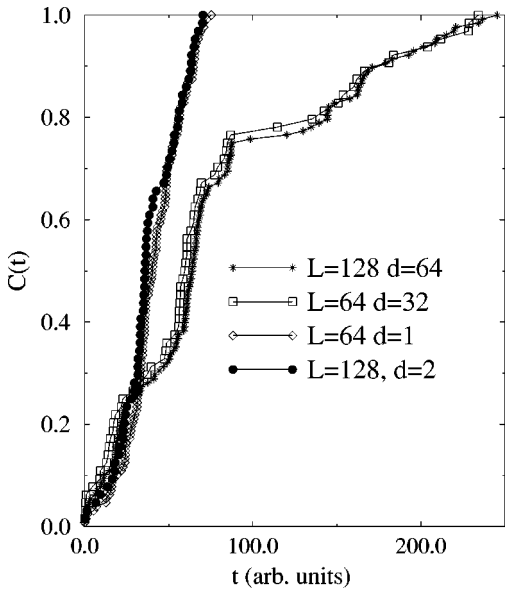

FIG. 3. Test of the geometrical finite size effects on tracer curves. Different tracer curves have been calculated for two different relative displacement of the joint ($\diamond$, $d/L=32/64=1/2$; $\bullet$, $d/L=64/128=1/2$ and $\square$, $d/L=1/64$; $\star$, $d=2/128$) and different domain size. The finite size effect influence on the dispersion coefficient estimation is smaller than 2% in each case.

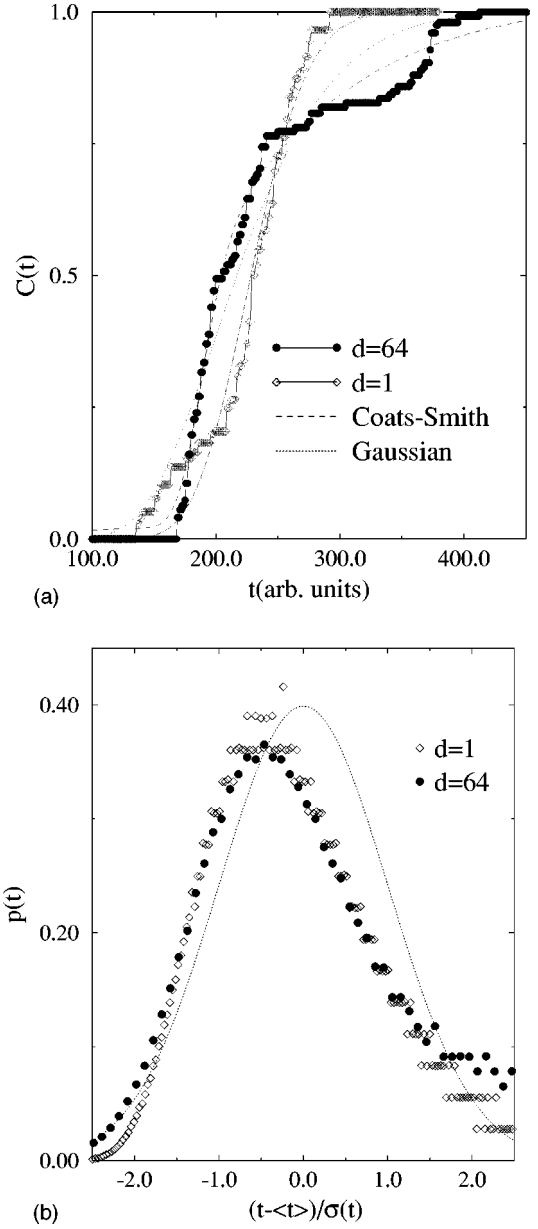

FIG. 4. (a) Dispersion curves for a 128×128 simulated crack for two different relative joint shifts d with the same fractured surface topography: $\bullet$, $d=64$; $\diamond$, $d=1$. Gaussian and Coats-Smith best fits are given for comparison, illustrating the non-Gaussian characteristics of dispersion. (b) Probability density function of the centered-reduced exit time corresponding to the numerical results in (a). A comparison with the dotted centered-reduced Gaussian distribution shows more clearly the non-Gaussian character of dispersion. The good superposition of the simulated curves indicates a small sensitivity of higher moments (>2) of the tracer exit time distribution to the typical correlation length of the crack.

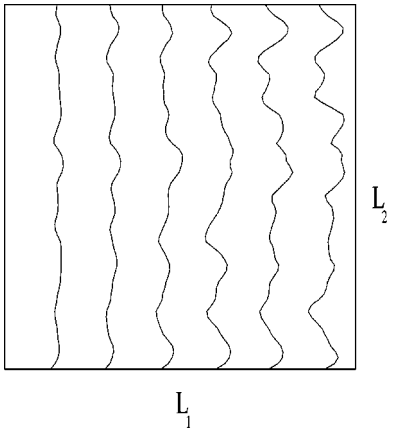

FIG. 5. For each sample we compute the isotime fronts at different mean traveled distances L_1: tracer locus front (isotime lines) and their growing roughness with the distance traveled in the (P,Ψ) coordinate system, for system size 128×128 with displacement $d=1$.

Figure 5 shows the spatial structure of tracer fronts, which is a single-valued function, for different mean advection times or, equivalently, different mean advected distances L_1. This figure displays a roughness of the front increasing along the transverse direction x_2 with the advection distance L_1 from the origin. Moreover, we see that the front roughness cannot be characterized by a single length scale. This qualitative picture will be fully compared to quantitative prediction of [16] in the following subsection.

Figure 6 illustrates the influence of the mean aperture h on the transit time distribution. This figure displays the sensitivity of dispersion curves with the aperture to one realization. A rescaling of transit time by a factor 4 permits a rough superposition of tracer curves corresponding to a factor 2 in the mean aperture h. The superposition between the data sets shown by closed circles and open diamonds indicates a decoupled effect of mean aperture h and relative translation d on the exit time distribution. Moreover, it shows a quadratic dependence of dispersivity with the mean aperture. The following subsection will study more precisely this decoupled influence on the averaged dispersivity.

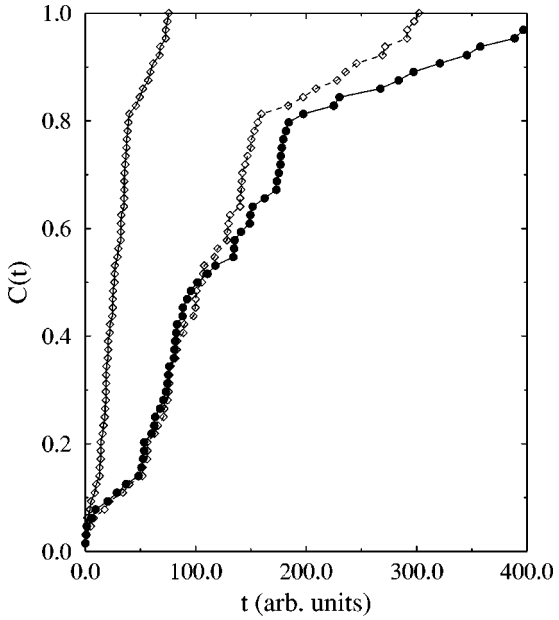

FIG. 6. Influence of the mean crack aperture on dispersion illustrated for two different gaps between the same crack faces, for a displacement $d=64$ and a domain size 128×128. The more open the crack, the more uniform the permeability and the velocity field and the less dispersion occurs. The straight line with ● corresponds to a $h=0.2$ gap, while ◇ is for $h=0.4$. The dotted line data set with ◇ corresponds to a linear time rescaling of the $h=0.4$ case by a factor 4.

C. Geometrical influence on global averaged dispersion

Statistical averaging is mandatory to analyze the mean influence on dispersion of the geometrical parameters. The simulations of Figs. 4(a) and 4(b) have shown how the two first tracer curve moments were sufficient to characterize the dispersion dependence on the typical correlation length d. Figure 7(a) shows the histogram of the probability density function (PDF) of numerically estimated dispersivity from 200 numerically generated dispersion curves. A broad distribution of dispersivity is observed, which increases with the relative shift d. A rescaling [Fig. 7(b)] permits us to obtain a good superposition between the different PDF's. This rescaling shows that the dependence of the first moment $\langle D\rangle$ on the relative shift d is sufficient to account roughly for the whole PDF. Some more refined simulations based on 1000 dispersion curves displayed in Fig. 7(c) illustrate the exponential tail of the dispersivity PDF.

A previous theoretical analysis [16], based on a simple first-order perturbation analysis such as the truncated equation (11) has quantified the anomalous dependence of the global dispersivity. In the limit $d\ll L_1, h\ll L_1$ the mean dispersivity $\langle D\rangle$ is expected to scale as

$$\langle D\rangle = \frac{A^2 L_1^{2\zeta-2}}{h^2}\, K(\zeta) d^2, \tag{22}$$

where h is the mean aperture, L_1 is the distance traveled in the mean flow direction, d is the shift between the aperture faces, A and ζ are, respectively, the roughness amplitude and exponent of the fracture surface, and $K(\zeta)$ is a parameter that depends on the orientation of the mean flow with respect to the relative shift direction $\vec{d}$ and on roughness exponent ζ. Figure 8(a) shows the mean dispersivity variation with the relative shift d/L for three different imposed mean apertures h while opening the crack from contact. The superposition of different curves in Fig. 8(b) rescaling the dispersivity by $1/h^2$ confirms the expected decoupling of the effects of mean aperture and relative shift indicated by Fig. 6 and predicted by Eq. (22). The quadratic dependence on d is also confirmed by numerical simulations. More precisely, the little difference observed between the expected quadratic behavior [dotted curves in Fig. 8(b)] and the numerical results may be due to a systematic finite size effect related to $O(d/L)$ corrections to Eq. (22). Anomalous dispersivity effects on the distance traveled L_1 are also a major feature of geometrical dispersion in rough self-affine cracks. This dependence comes from the wrinkling of the initially straight tracer line illustrated in Fig. 5. The front roughness $\sigma(L_1)$, the rms of the fluctuations, is exactly related to time fluctuations

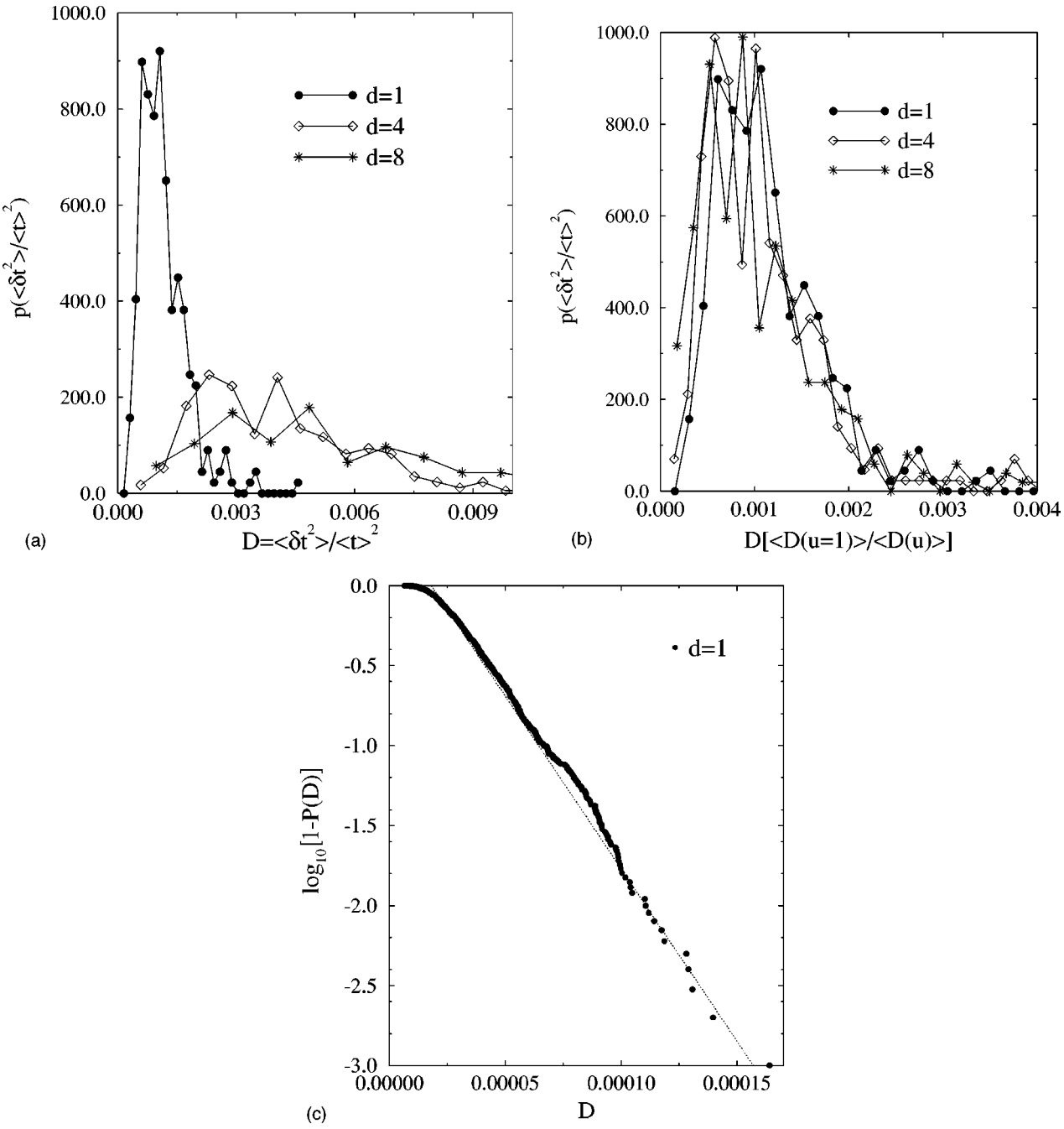

FIG. 7. Normalized histograms of the dispersivity computed from statistically generated dispersion curves. (a) PDF $p(D)$ of normalized dispersivity D for 200 generated crack topographies Broad variations of D that increase with the displacement d are observed: ●, $d=1$; ◇, $d=4$; ⋆, $d=8$ (the same seeds have been used for each displacement). (b) The rescaled dispersivity histograms shows a good superposition. The first moment of the dispersivity PDF is the relevant parameter to account for crack relative shift u. (c) Inverse cumulated dispersivity PDF obtained from 1000 realizations in the case $d=1$ (●). The dotted line indicates the exponential tail of the distribution.

$\sigma(L_1)=U\sqrt{\Delta T^2}$. Following Eqs. (21) and (22) and $T=L_1U$, the expected scaling of the front roughness is $\sigma(L_1)=U\sqrt{\Delta T^2}\propto L_1^{\zeta}$. Figure 9 displays variations of the front roughness with distance traveled L_1 computed numerically, showing a power law behavior coherent with the expected scaling. The observed small deviation from the expected $\zeta=0.8$ exponent is compatible with finite size effects as discussed in [30]. Thus anomalous dispersion occurs in the geometrical dispersion regime due to the long-range correlation of fracture roughness leading to an apparently *hyperdiffusive* process. The roughness of tracer front is directly related to the roughness exponent of the crack faces.

D. Anisotropy of the tracer front and consequences for dispersion

1. Anisotropy of macroscopic dispersion

We estimate quantitatively in this section the global dispersion anisotropy coming from the previously defined prefactor $K(\zeta)$. It is interesting to write from [18] the following

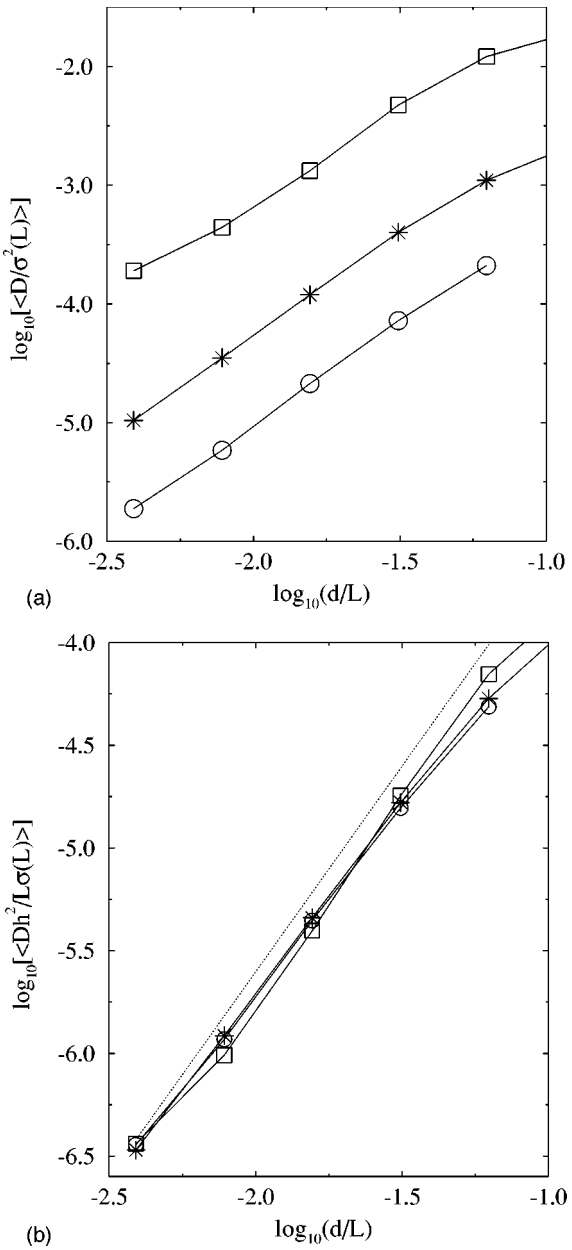

FIG. 8. (a) Mean dispersivity $\langle D \rangle$ variations with the crack relative shift d/L for three different mean apertures h: $h=0.2$ ($\square$), $h=0.5$ ($\star$); $h=2$ ($\bigcirc$) in arbitrary units, for a system size $L=256$, averaged over 30 samples. Dispersivity increases with d/L and decreases with the mean aperture h of the crack. (b) The rescaling $\langle Dh^2 \rangle$ shows a very good superposition. The mean aperture and relative shift dependence of $\langle D \rangle$ are thus decoupled. Moreover, (a) and (b) show the scaling of $\langle D \rangle$ as d^2.

expression for the aperture covariance, which has been computed analytically and shown in Fig. 3:

$$\mathrm{Cov}(\vec{x}) = \frac{|\vec{d}+\vec{x}|^{2\zeta} + |\vec{d}-\vec{x}|^{2\zeta} - 2|\vec{x}|^{2\zeta}}{2|\vec{d}|^{2\zeta}}. \tag{23}$$

At large scales $x \gg d$ this expression becomes

$$\mathrm{Cov}(\vec{x}) \sim 2\zeta \left\{ 1 + 2(\zeta-1)\left(\frac{\vec{x}\cdot\vec{d}}{|\vec{x}|\ |\vec{d}|} \right)^2 \right\} \left(\frac{|\vec{x}|}{|\vec{d}|} \right)^{-2(1-\zeta)}. \tag{24}$$

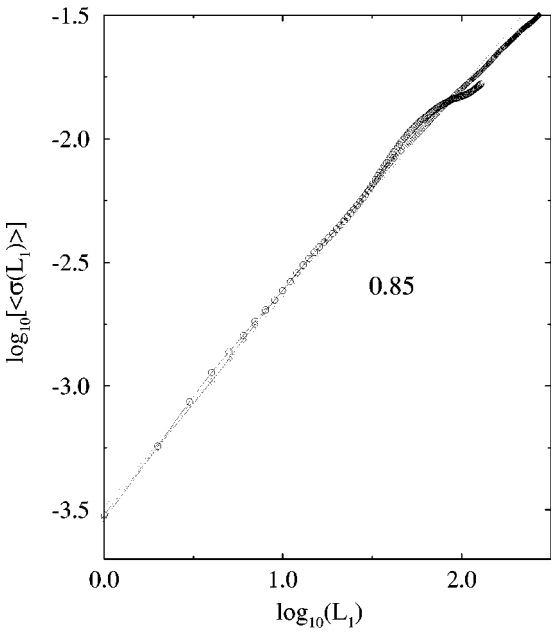

FIG. 9. Tracer locus front roughness dependence with the distance traveled L_1 is numerically studied for system sizes $L=256$ and 512, respectively averaged over 30 and 10 realizations, respectively. Root mean square time fluctuations $\sigma(L_1)$ are represented versus the mean distance traveled L_1 in log-log coordinates and display a clear power law behavior $\sigma(L_1) \propto L_1^{0.85}$. This small deviation from the expected $\zeta=0.8$ exponent is compatible with finite size effects as discussed in [30].

Using classical weak disorder expansions of [31,8,32], one can estimate the dispersion coefficient by computing the integral of the velocity covariance tensor projected along streamlines. A first estimate of such an integral is given by the simple integration of the aperture covariance, along straight lines. In this context, the dispersion coefficient integral is dominated by the long-range behavior of Eq. (24) in the case of persistent geometries, $1/2<\zeta<1$. Hence the anisotropy ratio of dispersion is simply given by the ratio of prefactors. In the case of mean imposed flow, parallel or perpendicular to the translation direction $\vec{d}$, one gets the anisotropy ratio

$$D_\parallel / D_\perp \simeq 2\zeta - 1. \tag{25}$$

This simple result, albeit obtained with a crude approximation, gives a qualitative picture of the anisotropy, showing increasing anisotropy as ζ goes to the value 1/2. In the same context of a long-wavelength expansion, from a Fourier description of the velocity fluctuations we obtain [16] the following integral dependence for orientational prefactors in Fourier space and radial coordinates

$$\begin{aligned} K_\parallel(\zeta) &\equiv \int\int k_\parallel(r,\theta) dr\ d\theta \\ &\equiv \int\int 2[1-\cos(r\ \cos\ \theta)] r^{-1-2\zeta} \\ &\quad \times [\cos(\theta)^2 - 2\sin(\theta)^2]^2 dr\ d\theta, \end{aligned} \tag{26}$$

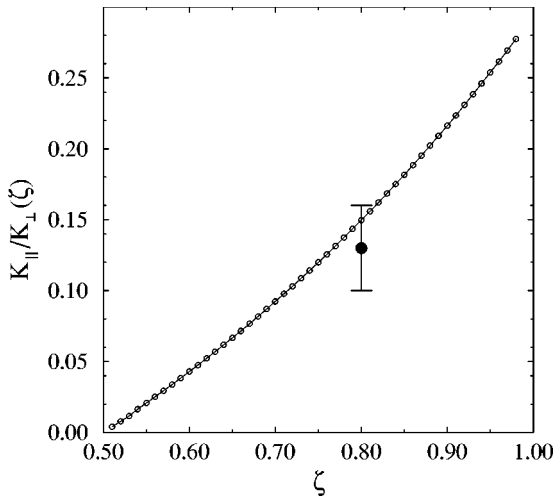

FIG. 10. Anisotropy ratio of dispersivity $K_{\perp}(\zeta)/K_{\|}(\zeta)$ estimated for the mean imposed flow parallel and perpendicular to the relative shift direction $\vec{d}$ ($\diamond$). Numerical calculations derived from an analysis of [16] is compared to numerical simulations results in the case $\zeta=0.8$ for 512×512 systems averaged over 10 realizations ($\bullet$). Both estimates are consistent, within error bars, indicating a strong anisotropy ratio of natural fractures.

$$K_{\perp}(\zeta)\equiv\int\int k_{\perp}(r,\theta)dr\ d\theta\equiv\int\int k_{\|}(r,\theta)\tan^2(\theta)dr\ d\theta.$$

The ratio of these parameters is displayed in Fig. 10; technical details about their computation are discussed in the Appendix. Comparing Fig. 10 and the previous rapid estimation (25), one can note the qualitative analogy showing a divergence of the anisotropy as ζ goes to 1/2. It is worth noting that this divergence is physically controlled by the system size in real cases while Eq. (26) is written in the case of infinite systems. Moreover, our numerical computation of the anisotropy from Eq. (26) displayed in Fig. 10 for $\zeta>1/2$ leads to stronger effects than expected from Eq. (25). In the special case of interest for many natural fractures $\zeta=0.8$, the prediction is $K_{\perp}(0.8)/K_{\|}(0.8)=6.68\pm0.01$. Direct numerical results are consistent with such a mean estimate of the anisotropy ratio $\langle D_{\perp}\rangle/\langle D_{\|}\rangle$ as shown in Fig. 10. Such a strong effect is experimentally interesting because it offers a unique opportunity to access the relative shift orientation from a tracer dispersion analysis.

2. Tracer front self-affine structure

Another interesting aspect of the anisotropy lies in the front structure itself. As mentioned previously, the meandering of the tracer line is of special interest for local dispersion. We are interested in the tracer meandering front that is a consequence of a weakly disordered permeability field. Let us note that the time needed to travel a distance L_1 along the flow (direction x_1) is

$$t(L_1,x_2)=\frac{1}{|v^{(0)}|}[L_1-\phi(L_1,x_2)], \tag{27}$$

where $\phi(L_1,x_2)$ is the transit time fluctuations and can be computed in Fourier space. We obtain in [16] the scaling behavior for long wavelengths $\vec{k}\vec{d}\ll1$,

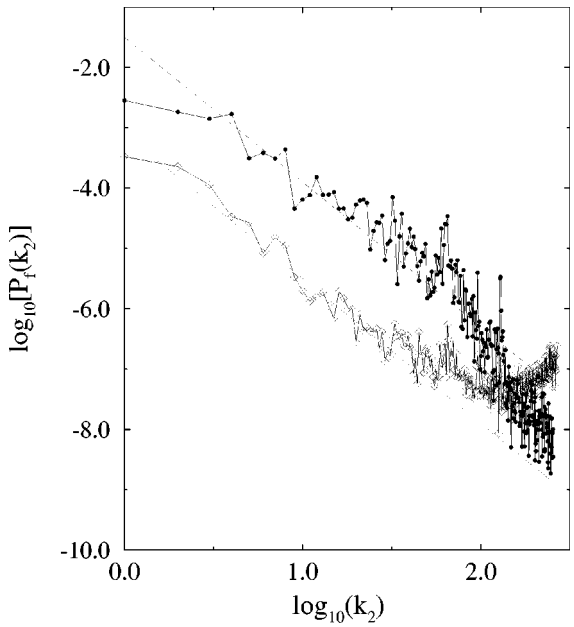

FIG. 11. Mean Fourier spectra $P_f(k_2)$ of the tracer front along the x_2 direction perpendicular to the mean flow. The average is performed over 10 realizations of 512×512 system size. $d=d_2=1$ ($\bullet$) and $d=d_1=1$ ($\diamond$) displacements perpendicular and parallel to the mean flow orientation are represented.

$$\tilde{\phi}(k_1,k_2)\propto-\frac{A}{h}\frac{\vec{k}\vec{d}\ \ |k|^{-1-\zeta}}{k_1}\left(\frac{k_1^2-2k_2^2}{k^2}\right). \tag{28}$$

A constant t section thus provides the geometry of this tracer line. Due to the perturbative origin of this result, a delay ϕ/v^0 can also be interpreted as a distance ϕ with respect to the mean front position. The function ϕ thus gives the progressive wrinkling of the tracer line. The most important property to be noted is the homogeneity of $\tilde{\phi}$ in k of degree $-(1+\zeta)$. Therefore, ϕ is a self-affine function of exponent ζ and the angular dependence in $\vec{k}$ space is to be interpreted as a significant anisotropy but does not change the roughness exponent. Therefore, we conclude that the front progressively develops a self-affine character over a range of scales that is limited by a short-range one d equal to the relative surface shift and a large one L_1, i.e., the convected distance.

We consider numerically the two cases where the relative shift between the two surfaces is either parallel or perpendicular to the mean flow direction, i.e., $\vec{d}=d\vec{e}_1$ and $\vec{d}=d\vec{e}_2$. Figure 11 shows the resulting power spectra of the front position with a power law fit corresponding to a determined roughness exponent $\zeta_{front}\approx0.75\pm0.10$, close to the choosen roughness exponent $\zeta_{surface}=0.8$. Thus the agreement with the theoretical prediction is quite satisfactory. In this figure the fracture surface is discretized on a 512×512 grid, the relative shift magnitude is 1, and L_1 is 256. The relative amplitude of the power spectra depending on the orientation of $\vec{d}$ for small k_2 gives the large-scale dispersion anisotropy displayed in Fig. 10.

IV. CONCLUSION

We have numerically analyzed dispersion in self-affine rough cracks in the geometrical regime, focusing on the de-

pendence of dispersion on simple geometrical parameters of natural fractures in this regime. We demonstrate numerically the significance of mean dispersivity with ensemble averaged simulations, which account for most of the observed tracer spreading dependence on geometrical parameters. We verified numerically previous theoretical predictions of the dispersivity dependence on the mean aperture, relative shift, and tracer traveling length of self-affine rough cracks. Anomalous dispersion and tracer front mean meandering variations as a function of advected distance have been considered in detail. Strong anisotropic effects have also been identified, even though the original fractured surface are statistically isotropic. Macroscopic dispersion anisotropy has been studied with both direct numerical simulation and analytic computations using an earlier large-scale perturbative expansion. Agreement is found between both approaches, indicating a large anisotropy ratio for the dispersivity coefficient in natural fractures. Moreover, this anisotropy has been shown to increase drastically as the crack roughness exponent ζ approaches 1/2. We thus quantified numerically the self-affine features of the tracer front, showing that its roughness exponent is simply equal to that of the crack face for all orientations of the flow. Moreover, a strong anisotropy is observed for the amplitude of the front roughness. This study motivates further experimental work on natural systems to examine and characterize the geometrical dispersion regime.

ACKNOWLEDGMENTS

We wish to thank R. Lenormand for pointing out interesting references and E. G. Flekkøy, R. Monasson, and A. Steyer for stimulating discussions. This work has been conducted with the support of a NATO Collaborative Research Grant between the City College of New York and ESPCI.

APPENDIX: NUMERICAL ESTIMATE OF ORIENTATIONAL EFFECTS

We analyzed in [16] the expression, in Fourier space, of orientational prefactor, in radial coordinates:

$$K_{\parallel}(\zeta)=\int\int k_{\parallel}(r,\theta)dr\ d\theta$$

$$=\int\int 2[1-\cos\ (r\ \cos\ \theta)]r^{-1-2\zeta}[\cos\ (\theta)^2$$

$$-2\sin\ (\theta)^2]^2 dr\ d\theta, \tag{A1}$$

$$K_{\perp}(\zeta)=\int\int k_{\parallel}(r,\theta)\tan^2(\theta)dr\ d\theta=\int\int k_{\perp}(r,\theta)dr\ d\theta. \tag{A2}$$

The above expression for $K_{\parallel}$ is convergent for $0<\zeta<1$ [one can easily check that for small distances $r\cos(\theta)\ll 1$ a Taylor expansion of the cosine provides an r^2 factor that guarantees the convergence of the above-mentioned integral]. The perpendicular dispersion integral involves an additional singularitiy for $r\to\infty$ and $\theta=\pi/2$. The latter singularity is, however, integrable if $\zeta>1/2$. For a smaller value of the roughness exponent, the divergence means physically that the integral is controlled by its upper bound (the distance traveled in this case) and thus the ratio of perpendicular to parallel dispersion coefficients becomes system size dependent. For $\zeta>1/2$ the integrals are all convergent and thus the anisotropy is finite and system size independent. The specific sensitivity of the dispersion coefficient to the orientation of the relative shift of the two surfaces with respect to the mean flow orientation is much more than a mathematical subtlety since it provides a potential access to the shift orientation from directional dispersion measurements in an open crack. This idea is discussed in more detail in the main text.

[1] K. J. Evans, T. Kohl, R. J. Hopkirk, and L. Rybach (unpublished).
[2] M. Sahimi, *Flow and Transport in Porous Media and Fractured Rocks*, (VCH, Weinheim, 1995).
[3] J. P. Bouchaud, E. Bouchaud, G. Lapasset, and J. Planès, Phys. Rev. Lett. **71**, 2240 (1993).
[4] S. Roux, J. Schmittbuhl, J. P. Vilotte, and A. Hansen, Europhys. Lett. **23**, 277 (1993).
[5] Y. W. Tsang and C. F. Tsang, Water Resour. Res. **25**, 2076 (1989).
[6] S. R. Brown, J. Geophys. Res. B **92**, 1337 (1987).
[7] J. Bear, *Dynamics of Fluids in Porous Media* (Elsevier, Amsterdam, 1972).
[8] L. W. Gelhar and C. L. Axness, Water Resour. Res. **19**, 161 (1983).
[9] F. Plouraboué, P. Kurowski, J. M. Boffa, J. P. Hulin, and S. Roux (unpublished).
[10] N. Huit, AIChE. J. **2**, 259 (1956).
[11] L. Moreno, L. Tsang, Y.W. Tsang, C.F. Hale, and F.V. Neretniek, Water Resour. Res. **24**, 2033 (1988).
[12] D. L. Koch and J. F. Brady, J. Fluid Mech. **154**, 399 (1985).
[13] G. I. Taylor, Proc. R. Soc. London, Ser. A **219**, 186 (1953).
[14] R. Aris, Proc. R. Soc. London, Ser. A **235**, 65 (1956).
[15] P.G. Saffman, J. Fluid Mech. **6**, 321 (1959).
[16] S. Roux, F. Plouraboué, and J. P Hulin, Transp. Porous Media (to be published).
[17] I. Ippolito, G. Daccord, E.J. Hinch, and J.P. Hulin, J. Contam. Hydrol. **16**, 87 (1994).
[18] F. Plouraboué, P. Kurowski, J. P. Hulin, S. Roux, and J. Schmittbuhl, Phys. Rev. E **51**, 1675 (1995).
[19] J. Schmittbuhl, S. Gentier, and S. Roux, Geophys. Res. Lett. **20**, 639 (1993).
[20] F. Plouraboué, K. Winkler, L. Petitjean, J. P. Hulin, and S. Roux, Phys. Rev. E **53**, 277 (1996).
[21] J. Koplik, I. Ippolito, and J. P. Hulin, Phys. Fluids A **5**, 1333 (1993).
[22] R. Gutfraind, I. Ippolito, and A. Hansen, Phys. Fluids **7**, 1938 (1995).

[23] M. E. Thompson, J. Geophys. Res. **96**, 4157 (1991).
[24] S. R. Brown, Geophys. Res. Lett. **13**, 1430 (1986).
[25] R. F. Voss, in *Fundamental Algorithms in Computer Graphics*, edited by R. A. Earnshaw (Springer-Verlag, Berlin, 1985), pp. 805–835.
[26] B. B. Dykaar and P. K. Kitanidis, Water Resour. Res. **28**, 1155 (1992).
[27] G. Matheron, *Eléments Pour une Théorie des Milieux Poreux* (Masson, Paris, 1967).
[28] M. E. Thompson, S. R. Brown, J. Geophys. Res. **96**, 21 923 (1991).
[29] K.H. Coats and B. D. Smith, Soc. Pet. Eng. J. Trans AIME **23**, 73 (1964).
[30] J. Schmittbuhl, J. P. Vilotte, and S. Roux, Phys. Rev. E **51**, 131 (1995).
[31] M. Avellaneda and A. J. Majda, Phys. Rev. Lett. **68**, 3028 (1992).
[32] R. Lenormand, Transp. Porous Media **18**, 245 (1995).